Applied Catalysis A: General 363 (2009) 221–229

Contents lists available at ScienceDirect

Applied Catalysis A: General

journal homepage: www.elsevier.com/locate/apcata

AgBr-Ag-Bi_2WO_6 nanojunction system: A novel and efficient photocatalyst with double visible-light active components

Lisha Zhang [a], Kin-Hang Wong [a], Zhigang Chen [b], Jimmy C. Yu [c,d], Jincai Zhao [e], Chun Hu [f], Chiu-Yeung Chan [g], Po-Keung Wong [a,d,*]

[a] Department of Biology, The Chinese University of Hong Kong, Shatin, NT, Hong Kong SAR, China
[b] State Key Laboratory for Modification of Chemical Fibers and Polymer Materials, College of Materials Science and Engineering, Donghua University, China
[c] Department of Chemistry, The Chinese University of Hong Kong, Shatin, NT, Hong Kong SAR, China
[d] Environmental Science Programme, The Chinese University of Hong Kong, Shatin, NT, Hong Kong SAR, China
[e] Center for Molecular Science, Institute of Chemistry, The Chinese Academy of Sciences, Beijing 100080, China
[f] Research Center for Eco-Environmental Sciences, The Chinese Academy of Sciences, Beijing 100085, China
[g] Department of Microbiology, The Chinese University of Hong Kong, Shatin, NT, Hong Kong SAR, China

ARTICLE INFO

Article history:
Received 3 March 2009
Received in revised form 4 May 2009
Accepted 12 May 2009
Available online 20 May 2009

Keywords:
AgBr-Ag-Bi_2WO_6
Nanojunction
Double visible-light active
Photocatalysis

ABSTRACT

A semiconductor-based photocatalyst system, consisting of two visible-light-driven (VLD) components and one electron-transfer system, has a great potential to efficiently photocatalytically degrade pollutants. In this paper, we have reported a simple strategy for constructing an all-solid-state AgBr-Ag-Bi_2WO_6 nanojunction by a facile deposition-precipitation method with Bi_2WO_6 as the substrate. Two visible-light active components (AgBr, Bi_2WO_6) and the electron-transfer system (Ag) are spatially fixed in this nanojunction system. Due to the presence of double visible-light active components, such a AgBr-Ag-Bi_2WO_6 nanojunction system has the broadened visible-light photo-response range, and it also exhibits higher photocatalytic activity than photocatalysts containing single visible-light active component, such as Bi_2WO_6, Ag-Bi_2WO_6 and AgBr-Ag-TiO_2 composite, for the degradation of the azo dye, Procion Red MX-5B and colorless pollutant pentachlorophenol. In addition, the initial dye concentration and pH value could greatly affect its photocatalytic activity, and the recycling experiments confirm that it is essentially stable during the photocatalytic process. In particular, the photocatalytic activity of AgBr-Ag-Bi_2WO_6 nanojunction is superior to the sum of the activities of two individual photocatalysts (AgBr-Ag-TiO_2 and Bi_2WO_6) that contain the same weight of AgBr or Bi_2WO_6, indicating the presence of a synergic effect between two visible-light active components in AgBr-Ag-Bi_2WO_6 nanojunction. On the basis of the photocatalytic results and energy band diagram, the photocatalytic process that may have occurred on the AgBr-Ag-Bi_2WO_6 nanojunction system is proposed; the vectorial electron transfer driven by the two-step excitation of both VLD components (AgBr and Bi_2WO_6) contributes to its high photocatalytic activity. Therefore, this work provides some insight into the design of novel and efficient photocatalysts with multi-visible-light active components for enhancing VLD photocatalytic activity.

1. Introduction

Environmental problems associated with harmful organic pollutants in water are the driving forces for sustained fundamental and applied research in the area of environmental remediation. Semiconductor photocatalysis offers a "green" technology for completely eliminating all kinds of contaminants, especially some azo dyes [1]. To date, the semiconductor TiO_2 has undoubtedly proven to be one of the most excellent photocatalysts for the oxidative decomposition of many organic compounds [2]. Unfortunately, due to its wide band-gap of 3.2 eV, TiO_2 can only be excited by ultraviolet or near-ultraviolet radiation, which occupies only about 4% of the solar light spectrum [3]. In order to efficiently utilize solar light in the visible region ($\lambda > 400$ nm) which covers the largest proportion of the solar spectrum, the development of visible-light-driven (VLD) photocatalysts has attracted a tremendous amount of attention.

Generally, two main synthesis strategies have been investigated for the preparation of VLD photocatalysts. One strategy is to extend the photo-response of TiO_2 to the visible region by doping of a non-metal or a transition metal such as $TiO_{2-x}N_x$ [4], $TiO_{2-x}S_x$ [5] and Fe/TiO_2 [6]. The other strategy involves exploiting novel VLD photocatalysts such as simple oxides and sulfides (Cu_2O [7] and CdS [8], respectively), complex oxides ($BiVO_4$ [9], $In_{1-x}Ni_xTaO_4$

* Corresponding author. Tel.: +852 2609 6383; fax: +852 2603 5767.
E-mail address: pkwong@cuhk.edu.hk (P.-K. Wong).

0926-860X/$ – see front matter © 2009 Elsevier B.V. All rights reserved.
doi:10.1016/j.apcata.2009.05.028

[10] and $PbBi_2Nb_2O_9$ [11]) and ternary sulfides [12]. Recently, we have also prepared some simple/complex oxides, such as nano-Cu_2O/carbon nanotubes composites [13], Bi_2O_3 [14] and Bi_2WO_6 superstructures [15,16], as single-component VLD photocatalysts. Up to date, although efforts have been made to prepare many kinds of single-component VLD photocatalysts, there are still some drawbacks hindering their practical application, such as short photogenerated electron–hole pair lifetimes and the limited region of visible-light photo-response. To meet the requirements of future environmental and energy technologies, it is still necessary to design novel VLD photocatalyst systems to further improve photocatalytic efficiencies.

Recently, the coupling of semiconductors with other semiconductors and/or metal on the nanoscale has been reported to greatly improve their photocatalytic performances [17–19]. For example, the deposition of a metal, such as Ag, on the surface of TiO_2 highly improved its photocatalytic efficiency through the Schottky barrier conduction band electron trapping [17]. Also, a novel *p*-$CaFe_2O_4$/*n*-$PbBi_2Nb_{1.9}W_{0.1}O_9$ nanodiode has shown greatly enhanced photocatalytic activity because of the good separation of photoexcited electrons and holes [18]. Tada et al. [19] have revealed that CdS-Au-TiO_2 three-component nanojunction system exhibits a high photocatalytic activity, far exceeding those of the single- and two-component systems, as a result of vectorial electron transfer driven by the two-step excitation of TiO_2 and CdS. Hu et al. [20] also prepared AgBr-Ag-TiO_2 as VLD photocatalyst for the destruction of the organic pollutant and bacteria, where AgBr is the only VLD component and the metal Ag specie on the surface is probably contributing to enhancing the electron–hole separation and interfacial charge transfer. These studies demonstrate that the development of better VLD photocatalysts depends on a wide range of visible-light photo-responses and highly effective interfacial charge transfers.

In order to broaden the range of visible-light photo-response and improve the separation of photo-generated electron–hole pairs simultaneously, herein we construct the AgBr-Ag-Bi_2WO_6 nanojunction system, where both AgBr and Bi_2WO_6 are photochemical systems that can be excited by visible light, while Ag is used as the electron-transfer system. This all-solid-state AgBr-Ag-Bi_2WO_6 nanojunction system with double visible-light active component exhibits much higher VLD photocatalytic activity than the photocatalyst with single visible-light active component such as Bi_2WO_6 superstructures, Ag-Bi_2WO_6 and AgBr-Ag-TiO_2, for the degradation of an azo dye, Procion Red MX-5B and a colorless pollutant, pentachlorophenol.

2. Experimental

2.1. Preparation of catalysts

The flower-like Bi_2WO_6 superstructures were prepared by the hydrothermal method according to our previous report [15]. In a typical case, 0.98 g $Bi(NO_3)_3{\cdot}5H_2O$ was first dissolved in a 30 mL 3.65 mol L^{-1} nitric acid solution, and a 20 mL aliquot of 0.05 mol L^{-1} Na_2WO_4 solution was added dropwise into the above solution. Then, the pH value of the resulting suspension was tuned approximately 1. After being stirred for 12 h, the suspension was added into a 50 mL Teflon-lined autoclave to reach 80% of its total volume. The autoclave was then sealed in a stainless steel tank and heated at 160 °C for 24 h. Subsequently, the reactor was cooled to room temperature naturally, and the precipitation was washed with de-ionized water and dried at 80 °C in air.

The AgBr-Ag-Bi_2WO_6 nanojunction was prepared using the modified deposition-precipitation method [20,21]. The Bi_2WO_6 superstructure (0.9 g) as the substrate was added to 20 mL of distilled water, and the suspension was sonicated for 10 min. Then, 0.45 g of cetylmethylammonium bromide (CTAB) was added to the suspension, and the mixture was stirred magnetically for 30 min. Next, 0.105 g of $AgNO_3$ in 2 mL of NH_4OH (25 wt% NH_3) was quickly added to the mixture, and the resulting suspensions were stirred at room temperature for 24 h. The product was filtered, washed with water and dried at 70 °C. Finally, the powder was calcined in air at 500 °C for 3 h. For comparison, the as prepared Bi_2WO_6 superstructure was calcined at 500 °C for 3 h, a Ag-Bi_2WO_6 sample was prepared without the addition of CTAB, and another AgBr-Ag-TiO_2 sample was prepared using the same weight of titania P-25 as a substrate with other conditions identical.

2.2. Characterization of catalysts

The scanning electron microscope (SEM) characterizations were performed on an FEI QUANTA-400F field emission scanning electron microscope (Holland), while the transmission electron microscope (TEM) analyses were performed using a FEI TECNAI F20 field emission electron microscope (Holland) and the energy-dispersive X-ray analysis (EDXA) of the samples was also performed during the TEM measurements. Furthermore, the X-ray photoelectron spectroscopy (XPS) data were recorded with a Quantum 2000 scanning ESCA microprobe instrument (Φ Physical Electronics, USA) using monochromatic Al Kα radiation (225 W, 15 mA, 15 kV) with the spot size of 100 μm and low-energy electron flooding for charge compensation. To compensate for surface charges effects, we calibrated the binding energies using the C 1s hydrocarbon peak at 284.6 eV. The X-ray diffraction (XRD) patterns were recorded on a Huber diffractometer (V612365, Japan) that was equipped with a rotating anode using Cu Kα radiation (Rigaku, Ru-300) over the range of $20^\circ \leq 2\theta \leq 80^\circ$. Finally, the UV–vis absorption spectra of the samples were recorded on a UV–vis spectrophotometer (JASCO V-550, Japan) with an integrating sphere attachment. The zeta-potential of catalysts was measured by a zeta potential analyzer equipped with a data system of ZetaPlus 3.57 version and Model ZetaPlus (Brookhaven Instruments Corporation, NY, USA).

2.3. Photocatalytic degradation of MX-5B and PCP under visible light

Photocatalytic activities of the photocatalysts were evaluated by degrading Procion Red MX-5B (MX-5B, a monoazo dye) and pentachlorophenol (PCP), using a 300 W xenon lamp (Beijing Perfect Light Co. Ltd., Beijing) as light source. Light was passed through a UV cut-off filter (λ>400 nm), and then was focused onto a 100-mL beaker or flask containing MX-5B or PCP. In each experiment, a suitable amount of photocatalyst was added into MX-5B or PCP aqueous solution. Prior to irradiation, the suspensions were magnetically stirred in the dark for 60 min to ensure that an adsorption/desorption equilibrium was established between the photocatalyst and the target organic pollutant.

When the remaining MX-5B concentration needed to be measured, at given irradiation time intervals, 1.5 mL aliquots were collected, centrifuged, and then filtered through a Millipore filter (pore size 0.22 μm) to remove the catalyst particulates for analysis. The filtrates were analyzed by recording variations at the wavelength of maximal absorption in the UV–vis spectra of MX-5B with a UV-3600 (Shimadzu, Japan) spectrophotometer.

PCP concentration was determined by using reverse-phase high performance liquid chromatography (HPLC) described previously [22]. The analysis was performed by using a Waters 600 multi-solvent delivery system equipped with a Waters reverse-phase C18 (5 μm particle) column (4.6 mm × 250 mm, Waters Spherisorb®, Waters Corporation, Milford, Ireland) and a Waters 996 photodiode array detector. The mobile phase consisted of 75% acetonitrile, 24.875% Milli-Q water, and 0.125% acetic acid at a flow

rate of 1.5 mL min^{-1}. The maximum absorption wavelength was detected at 215 nm. Concentrations of PCP were calculated according to a standard curve obtained from HPLC measurements of the standard at different concentrations. The detection limit for PCP is around 0.5 mg L^{-1}.

Total organic carbon (TOC) analysis was carried out with a Shimadzu TOC-5000A total organic carbon (TOC) analyzer. After each desired reaction time, 20 mL of suspension was taken out and the catalyst was removed by filtering the suspension through a 0.2-μm filter membrane, then the filtrate was analyzed by the machine. For the detection of the evolved CO_2 and inorganic carbon (IC) concentration, the flask containing photocatalyst and MX-5B solution was first saturated by the N_2 gas before being closed, and then the closed system was irradiated under the visible light. After irradiation for the desired time, the gas in the reactor was pumped through the Kitagawa precision gas detector tubes for carbon dioxide (Komyo Rikagaku Kogyo K.K., Kawasaki, Kanagawa, Japan). The amount of the evolved CO_2 was determined by a degree of color-changed the CO_2 adsorbent in the tubes. The resulting liquid–solid mixture was immediately filtered and the solution phase was subjected to measurements of IC by the TOC analyzer.

3. Results and discussion

3.1. Preparation and characterization of catalysts

First, the Bi_2WO_6 sample was prepared by hydrothermal reaction under the acidic condition according to our recent report [15]. As shown in Fig. 1A, this sample exhibits flower-like superstructures, which are in fact built from two-dimensional nanoplates with a smooth surface (Fig. 1B). Subsequently, Ag/AgBr was deposited onto the Bi_2WO_6 substrate by impregnating the aqueous solution of $AgNO_3$ and NH_4OH to the aqueous solution containing Bi_2WO_6 substrate and CTAB via the modified deposition-precipitation method [20,21]. In this process, at alkaline condition, cationic surfactant CTAB could be adsorbed onto the

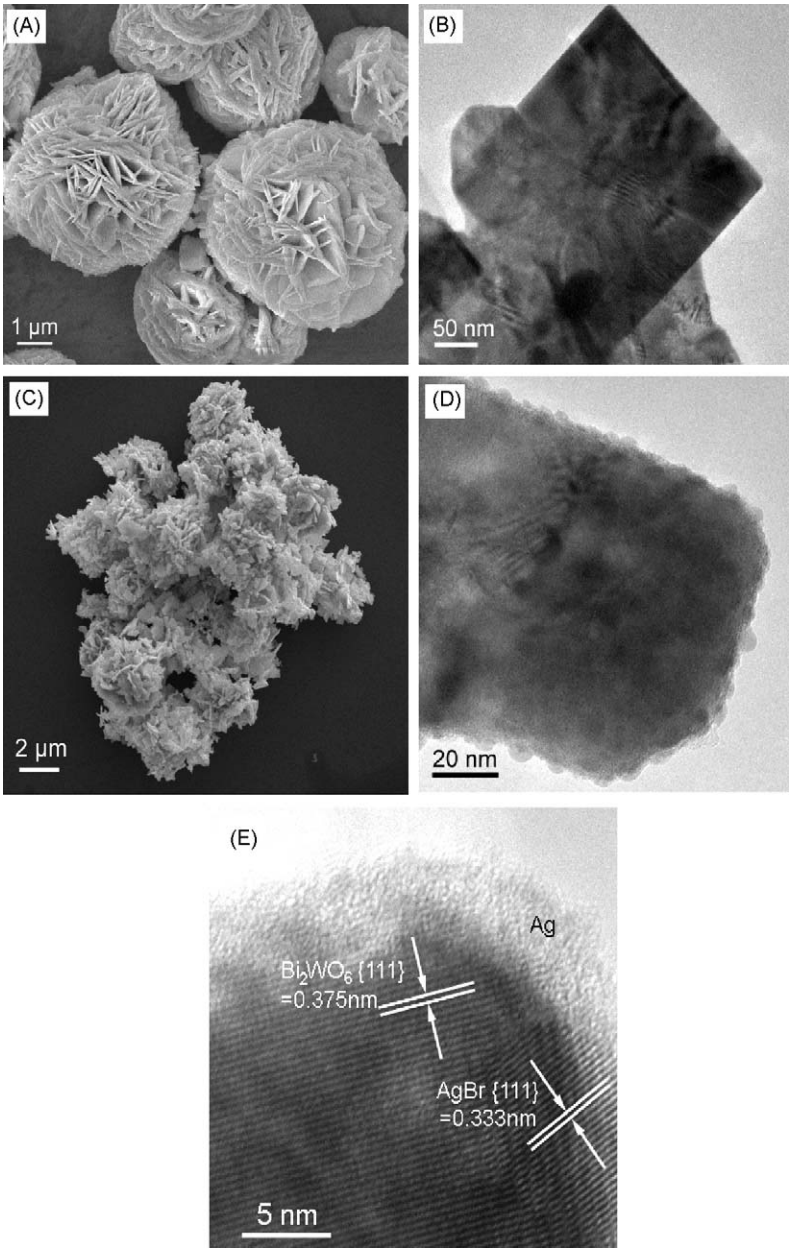

Fig. 1. SEM (A) and TEM (B) images of Bi_2WO_6 sample; SEM (C), TEM (D) and HR-TEM (E) images of AgBr-Ag-Bi_2WO_6 nanojunction system.

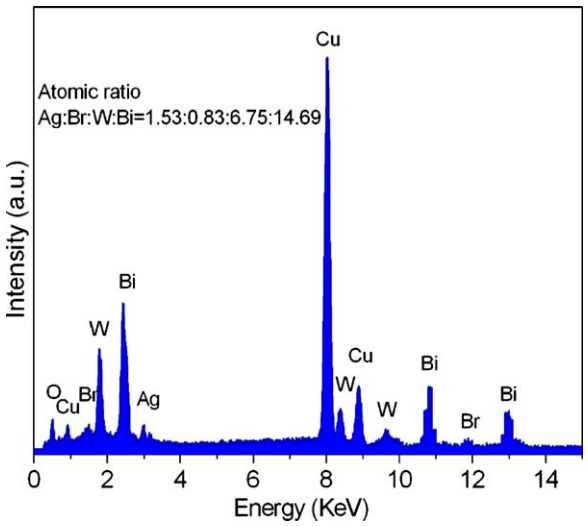

Fig. 2. EDXA spectra of AgBr-Ag-Bi_2WO_6 nanojunction system.

surface of Bi_2WO_6 to limit the number of nucleation sites where AgBr could grow, leading to homogeneously dispersed AgBr islands on the Bi_2WO_6 nanoplates. Aside from this, CTAB could supply bromide to precipitate Ag^+ in solution; however, it should be noted that metal Ag formation occurred along with the formation of AgBr [20,21]. After the deposition-precipitation process and subsequent calcination treatment (at 500 °C for 3 h), the Bi_2WO_6 superstructures are slightly disintegrated to form clusters of nanoplates (Fig. 1C). Interestingly, many nanoparticles with the mean size of 5 nm are firmly dispersed on the surface of the Bi_2WO_6 nanoplate, forming nanodimensional junctions, as demonstrated in TEM image (Fig. 1D). The HR-TEM image (Fig. 1E) of the sample further demonstrates that the lattice spacings of the two fixed components, determined to be 0.375 and 0.333 nm, are in good agreement with the values for the Bi_2WO_6 (1 1 1) plane (JCPDF No. 73-1126) and for the cubic AgBr (1 1 1) plane (JCPDF No. 79-0149), respectively. It can also be observed that the Bi_2WO_6 nanoplate is partially enwrapped in an amorphous nano-shell, where the AgBr crystalline is located beside it.

The compositions and the chemical state of its constituent elements of AgBr-Ag-Bi_2WO_6 nanojunction system as well as AgBr-Ag-TiO_2 composite were investigated by EDXA and XPS analysis (Figs. 2 and 3). (The EDXA spectrum of AgBr-Ag-TiO_2 was also attached in the supporting information as Fig. S1.) The EDXA spectrum reveals that, besides Bi, W, and O elements present from the Bi_2WO_6 substrate (Fig. 2), there are only Ag and Br elements, indicating the presence of AgBr and/or Ag in nanojunction system

Table 1
Weight percentage (%) of each component in the catalyst.

	Ag	AgBr	Bi_2WO_6 or TiO_2
AgBr-Ag-Bi_2WO_6	1.48	3.04	95.5
AgBr-Ag-TiO_2	0.874	2.74	96.4

(copper signals appear from the copper grid). More importantly, EDAX relies on the penetration depth of electrons with relatively high kinetic energetic and yields the composition of the material within a region approximately 1 μm below the surface [23]. It might contain information not only due to the nanoplate surface but also due to the core of the sample clusters. Thus the quantitative amount of components in the sample can be approximately estimated from the knowledge of the fraction of the elemental composition obtained from the EDAX analysis, as shown in Table 1. On the other hand, XPS is based on the limited escape depth of electrons with relatively low kinetic energy and reveals information on the topmost few angstroms of the surface [23]. Thus, it is appropriate for detecting valency states of elements on the surface. Fig. 3 show the high-resolution XPS spectra of the Ag 3d and Br 3d regions. The Ag $3d_{3/2}$ and Ag $3d_{5/2}$ peaks are identified at 374.0 and 368.0 eV, respectively, suggesting the presence of metal Ag (Fig. 3A) [20]. Moreover, the peak of Br 3d at 68.9 eV is due to the crystal lattice of Br in AgBr [24]. These results confirm that there are both Ag and AgBr species in the nanojunction system.

Subsequently, the phase of the AgBr-Ag-Bi_2WO_6 nanojunction system, as well as the Bi_2WO_6 sample, was investigated by XRD patterns (Fig. 4A and B). All samples exhibit some diffraction peaks that are assigned to the orthorhombic Bi_2WO_6 phase (JCPDF No. 73-1126) [15]. In addition, in the AgBr-Ag-Bi_2WO_6 nanojunction system, there are two peaks with 2θ values of 30.94° and 44.33° corresponding to (2 0 0) and (2 2 0) crystal planes of cubic AgBr (JCPDF No. 79-0149), respectively (Fig. 4B). Moreover, the diffraction peak (at 64.4°) assigned to metal Ag is also displayed in the nanojunction system (the inset of Fig. 4), and it is especially weak, indicating that Ag is poorly crystallized. These results are in good agreement with the HR-TEM analysis (Fig. 1E).

Based on the TEM, EDAX, XPS and XRD results demonstrated above, one can conclude that the amorphous nano-shell in Fig. 1E should be metal Ag. Therefore, the construction of an AgBr-Ag-Bi_2WO_6 nanojunction system is well established.

The optical absorptions of the Bi_2WO_6 sample and AgBr-Ag-Bi_2WO_6 nanojunction system were measured using an UV–vis spectrometer (Fig. 5). It is clear that the Bi_2WO_6 sample exhibits strong photoabsorption from the UV light region to visible light shorter than 470 nm, corresponding to the indirect band-gap of

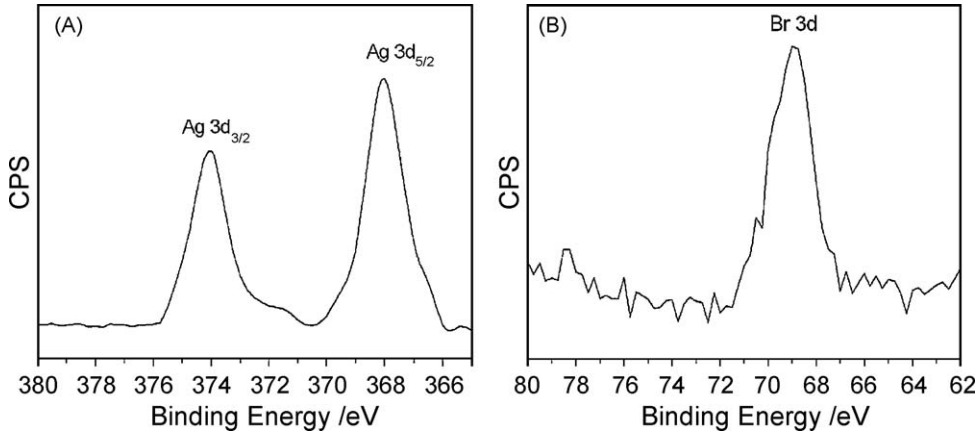

Fig. 3. Ag 3d (A) and Br 3d (B) XPS spectra of AgBr-Ag-Bi_2WO_6 nanojunction system.

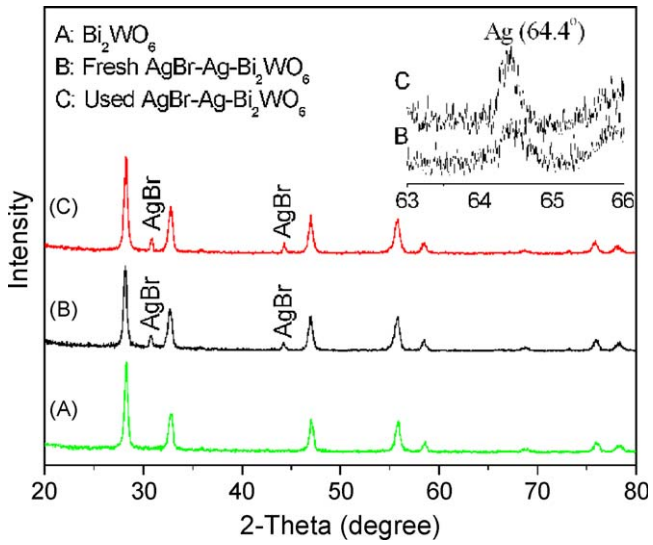

Fig. 4. XRD patterns of (A) Bi_2WO_6 sample, (B) the fresh AgBr-Ag-Bi_2WO_6 nanojunction, and (C) the used AgBr-Ag-Bi_2WO_6 nanojunction after photodegradation of MX-5B under visible-light irradiation. The insert shows peaks of Ag^0 in the fresh and used AgBr-Ag-Bi_2WO_6 nanojunction system.

Bi_2WO_6 [15]. Importantly, aside from the photoabsorption from Bi_2WO_6, the AgBr-Ag-Bi_2WO_6 nanojunction displays another wide yet weak absorption band around 450–700 nm, corresponding to the indirect band-gap of AgBr and surface plasmon absorption of metal Ag [20]. These facts indicate that the region of visible-light photo-response can be broadened by the conjunction of photo-absorption of visible-light active components, AgBr and Bi_2WO_6 in the AgBr-Ag-Bi_2WO_6 nanojunction system. Thus, VLD photocatalytic performance of AgBr-Ag-Bi_2WO_6 nanojunction system can be expected to be excellent compared with that of photocatalysts with single visible-light active components.

3.2. Photocatalytic performance under visible-light irradiation

MX-5B (Fig. 6), a common monoazo dye widely used in dyeing cellulose, nylon, silk and wool, was chosen as a representative pollutant to evaluate the photocatalytic performance of photocatalysts. When dissolved in distilled water, MX-5B displays a major

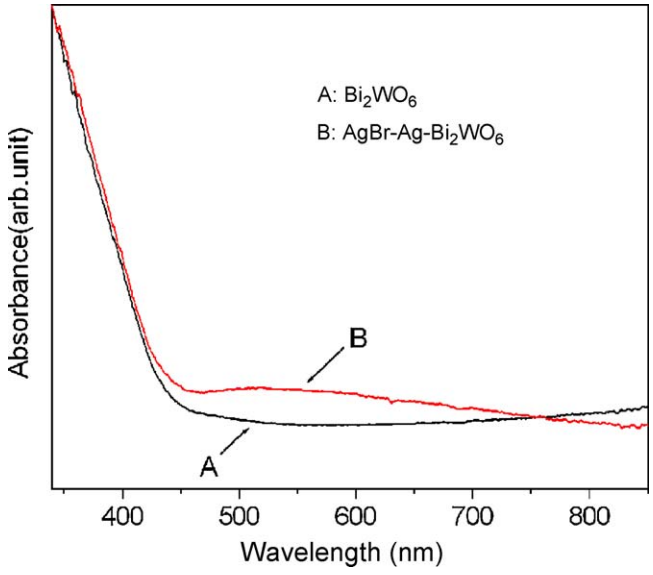

Fig. 5. UV–vis diffuse reflectance spectra of (A) Bi_2WO_6 sample and (B) AgBr-Ag-Bi_2WO_6 nanojunction system.

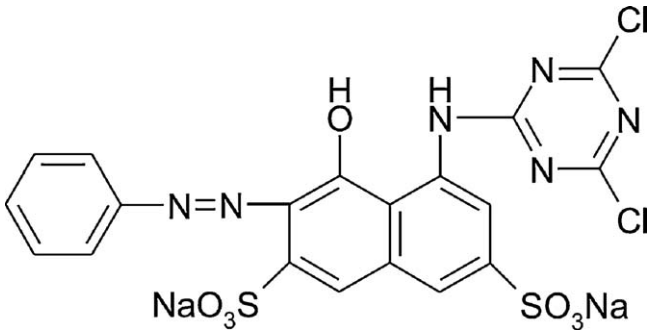

Fig. 6. The chemical structure of MX-5B.

absorption band centered at 538 nm that is used to monitor the photocatalytic degradation. Fig. 7 shows the adsorption and photodegradation of MX-5B by different photocatalysts containing the same weight of each visible-light-active component under visible-light irradiation ($\lambda \geq 400$ nm). As a comparison, MX-5B degradation without photocatalysts was also performed, and the results demonstrate that MX-5B is not degraded in the absence of photocatalyst under visible-light irradiation (Fig. 7A). The AgBr-Ag-TiO_2 composite shows the greatest adsorption of MX-5B in the dark, while the others have similar adsorption abilities as shown in Fig. 7.

Recently, we have showed that Bi_2WO_6 superstructures exhibited excellent photocatalytic activities under visible-light illumination for the degradation of Rhodamine B [15]. In this study, the concentration of MX-5B only had a drop of 2.0 mg L^{-1} when using Bi_2WO_6 superstructures as photocatalyst after 60 min of reaction time (Fig. 7B), since azo dyes (such as MX-5B) are usually more resistant to biological and chemical degradation than other dyes (such as Rhodamine B) [25]. Furthermore, the photocatalytic degradation can be elevated to 2.9 mg L^{-1} in the presence of Ag in Bi_2WO_6 superstructures (Fig. 7C) since the junction of metal Ag can improve the electron–hole separation and interfacial charge transfer [17,19–20]. When AgBr-Ag-TiO_2 composite with AgBr as single visible-light active component was used as the photocatalyst, the photocatalytic degradation of MX-5B reaches

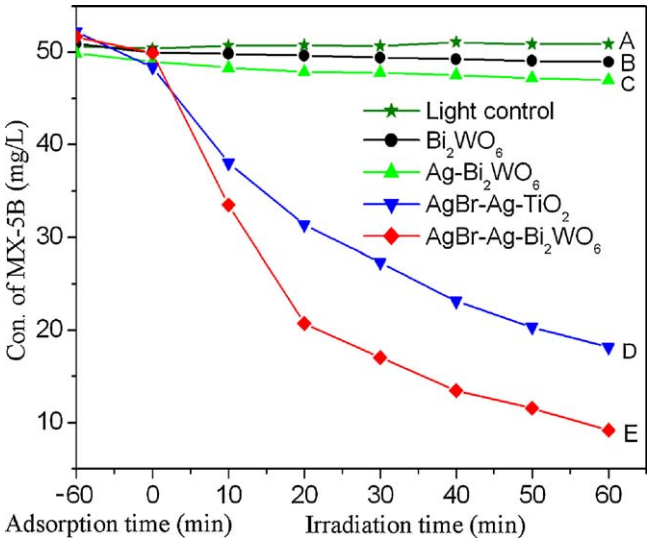

Fig. 7. The adsorption and photodegradation of MX-5B (50 mg L^{-1}, 100 mL, at natural pH of 6.5) by different photocatalysts with the same weight of each visible-light-active component under visible-light irradiation: (A) light control (without photocatalyst); (B) 47.8 mg Bi_2WO_6; (C) 48.5 mg Ag-Bi_2WO_6 containing 47.8 mg Bi_2WO_6; (D) 55.6 mg AgBr-Ag-TiO_2 composites containing 1.52 mg AgBr; (E) 50 mg AgBr-Ag-Bi_2WO_6 nanojunction containing 1.52 mg AgBr and 47.8 mg Bi_2WO_6.

34.1 mg L^{-1} after 60 min visible-light irradiation (Fig. 7D). Surprisingly, by AgBr-Ag-Bi_2WO_6 nanojunction system with two visible-light active components (AgBr and Bi_2WO_6), the MX-5B could be photocatalytically degraded 42.8 mg L^{-1} and the removing efficiency could reach 85% within 60 min under visible-light irradiation, indicating the highest photocatalytic activity (Fig. 7E). Based on the above results, it can be deduced that each component in the AgBr-Ag-Bi_2WO_6 nanojunction system is crucial for its excellent photocatalytic activity.

In addition, the degradation rate by AgBr-Ag-Bi_2WO_6 nanojunction system is much higher than that by AgBr-Ag-TiO_2 composite within the 20 min (Fig. 7D and E). The subsequent degradation rate of MX-5B by AgBr-Ag-Bi_2WO_6 nanojunction system decreases due to the following two reasons. Firstly, the concentration of MX-5B goes down, thus the vanishing rate reduces kinetically. Secondly, the intermediates formed upon photocatalytic oxidation of the parental dye, such as aromatics, aldehydes, ketones and organic acids as shown by previous studies [26,27], compete with the micro-molecular MX-5B in the degrading reaction.

Previous studies showed that, in the presence of photocatalysts (such as TiO_2), some organic dyes that absorb visible light could be degraded by sensitization mechanism [28–30], because the excited electrons of these dyes can inject into the conduction band of photocatalysts and subsequently these organic dyes are oxidized. In our case, however, the LUMO of MX-5B (−0.9 V versus NHE) [31] is more positive than the potential of conduction band of AgBr (−1.04 V versus NHE) [32]; thus, the excited electrons of dye are thermodynamically unfavorable to transfer to AgBr. Although the LUMO of MX-5B is more negative than the potential of conduction band of Bi_2WO_6 (−0.07 V versus NHE) [33], the Bi_2WO_6 show poor activity for the degradation of MX-5B as shown in Fig. 7B, which indicates that the charge injection from the MX-5B to the Bi_2WO_6 is inefficient. In order to further investigate the photodegradation of MX-5B, Fig. 8 illustrates the total organic carbon (TOC) removal efficiency, and formation of CO_2 and inorganic carbon (IC: HCO_3^- and CO_3^{2-}) during the mineralization of MX-5B by AgBr-Ag-Bi_2WO_6 nanojunction under visible-light irradiation. TOC removal efficiency increases to 61% after 28 h, accompanying a steady increase of the amount of evolved CO_2 and the concentration of IC in the solution as shown in Fig. 8. These results confirm that MX-5B is steadily mineralized by AgBr-Ag-Bi_2WO_6 nanojunction and that the loss of TOC is transformed to gaseous CO_2 and/or inorganic carbon in solution. Therefore, the effectively photocatalytic degradation of MX-5B by AgBr-Ag-Bi_2WO_6 (Fig. 7E) are mainly

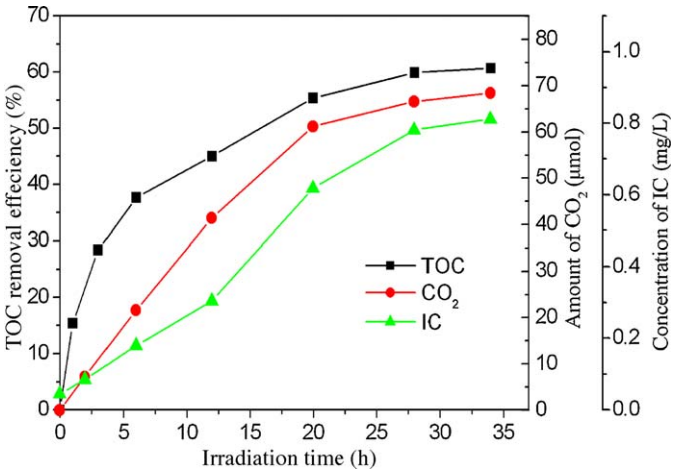

Fig. 8. The TOC removal efficiency, the evolved CO_2 and IC concentration during the MX-5B photodegradation process (40 mg L^{-1}, 200 mL) in aqueous dispersions with 0.4 g AgBr-Ag-Bi_2WO_6 nanojunction under visible-light irradiation.

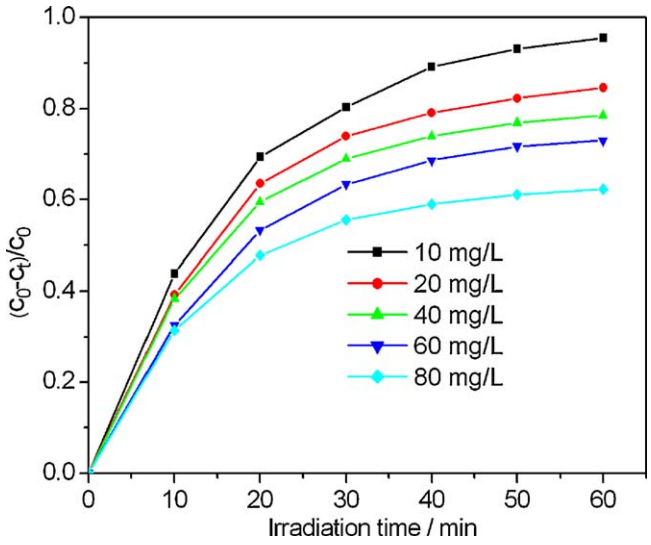

Fig. 9. The photocatalytic degradation of MX-5B by AgBr-Ag-Bi_2WO_6 nanojunction at various initial concentrations; 100 mL suspensions containing 25 mg photocatalyst, natural pH value of 6.5, $\lambda > 400$ nm.

derived form the direct bandgap excitation instead of sensitization mechanism. With prolonged irradiation time (>34 h), the TOC content of the solution could not be reduced further because the triazine group of MX-5B is converted to cyanuric acid (CA), which is very stable in photocatalysis [25].

The influence of the initial concentration of MX-5B on the photocatalytic rate was also investigated, and the results are shown in Fig. 9. Obviously, the photodegradation rate decreases with the increase of initial dye concentration. One possible reason for such a result is the visible-light screening effect of the dye itself. At a high dye concentration, a significant amount of visible light may be absorbed by the dye molecules rather than by the AgBr-Ag-Bi_2WO_6 nanojunction particles and thus the efficiency of the catalytic reaction is reduced. Another possible reason is the interference from intermediates formed during the photocatalytic oxidation process. They may compete with the dye molecules for the limited adsorption and catalytic sites on the photocatalytic particles [26] and thus inhibit decolorization. Such suppression would be even more pronounced in the presence of an elevated level of degradation intermediates formed upon an increased initial dye concentration.

With AgBr-Ag-Bi_2WO_6 nanojunction system as a photocatalyst, the effects of pH value of solutions on photodegradation efficiencies of MX-5B were studied as shown in Fig. 10. Obviously, the photodegradation efficiency goes up with the decrease of pH from 9 to 3. When the pH value is 3, the MX-5B could be photocatalytically degraded 40 mg L^{-1} using 25 mg AgBr-Ag-Bi_2WO_6 after 60 min of visible-light irradiation. As the adsorption of dye molecules onto the catalyst surfaces is an important step for photocatalytic oxidation (PCO) to take place, we further examined the relationship between pH value of the solution and the adsorption of MX-5B by AgBr-Ag-Bi_2WO_6 nanojunction, as shown in the inset of Fig. 10. The adsorption capability of MX-5B is found to increase with the decreasing pH from 9 to 3. Previous studies reveal that the adsorption and photodegradation of dye pollutants are pH-dependent, chiefly resulting from the variation of surface charge of catalysts with pH [34]. Here, the surface charge of AgBr-Ag-Bi_2WO_6 nanojunction at different pH values was investigated by the zeta potential test (Fig. 11). The result indicates that the zero point of charge is 3.7. The surface charge is positive when pH <3.7, and it becomes more negative with higher pH value when pH >3.7. In addition, the charge of MX-5B in aqueous solution is negative

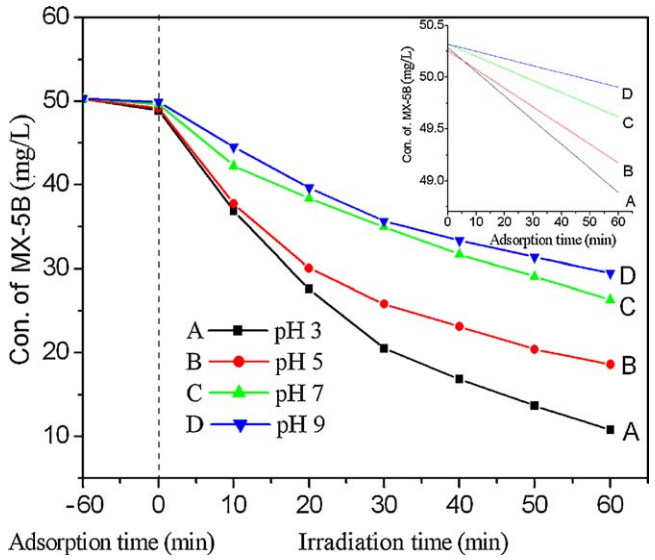

Fig. 10. The photodegradation of MX-5B (50 mg L^{-1}, 100 mL) in aqueous solutions with different initial pH values, containing 25 mg AgBr-Ag-Bi_2WO_6 nanojunction under visible-light irradiation. The effect of pH on the adsorption of MX-5B is shown in the inset of the figure.

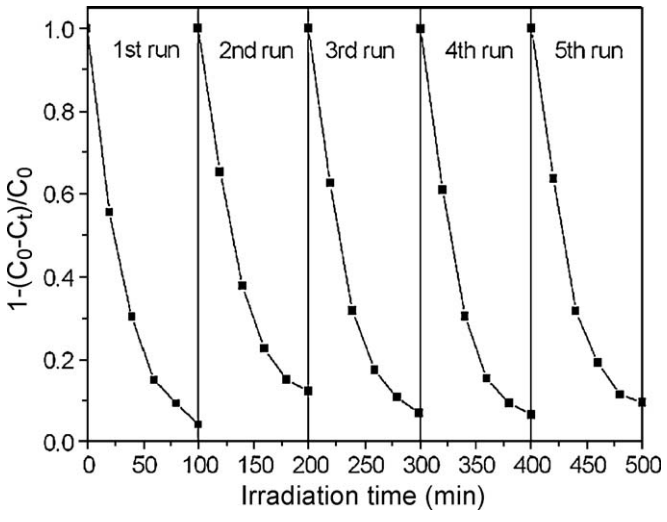

Fig. 12. Cycling runs in the photodegradation of MX-5B (50 mg L^{-1}, 100 mL) at natural pH of 6.6 in aqueous dispersions containing 50 mg of AgBr-Ag-Bi_2WO_6 nanojunction under visible-light illumination.

due to the presence of $-SO_3^-$ group (Fig. 6). Thus, electrostatic repulsion between the dye molecules and AgBr-Ag-Bi_2WO_6 nanojunction goes down with the decrease of pH from 9 to 3, resulting in the improvement of the adsorption and photodegradation of MX-5B.

The stability of the AgBr-Ag-Bi_2WO_6 nanojunction system was also studied through the degradation of MX-5B under visible-light irradiation (Fig. 12). It should be noted that the AgBr-Ag-Bi_2WO_6 nanojunction were easily recycled by simple filtration without any treatment in these experiments. After five cycles of the photodegradation process of MX-5B, the AgBr-Ag-Bi_2WO_6 nanojunction does not exhibit any significant loss of activity, as shown in Fig. 12, confirming that the components of the AgBr-Ag-Bi_2WO_6 nanojunction is not photocorroded and that the nanojunction structure is stable during the photocatalytic process. XRD patterns of the AgBr-Ag-Bi_2WO_6 nanojunction system before (Fig. 4B) and after (Fig. 4C) photocatalytic reaction also show that the crystal structures of different components have no obvious changes.

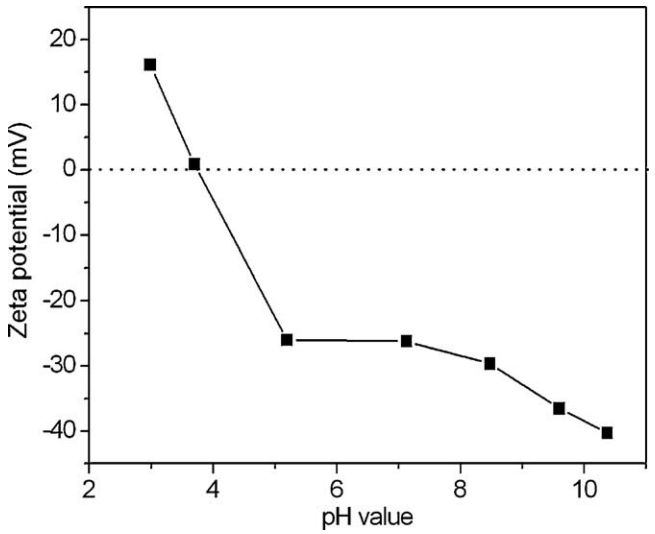

Fig. 11. Zeta potential for a suspension containing 0.05 g/L of AgBr-Ag-Bi_2WO_6 nanojunction in the presence of KNO_3 (10^{-4} M) at different pH value.

Although the single AgBr component is usually unstable under light irradiation, AgBr in the nanojunction system is not destroyed during the photocatalytic process, which results from the fact that the presence of metal Ag can inhibit the decomposition of AgBr under visible-light-irradiation conditions [20,21]. Therefore, the present AgBr-Ag-Bi_2WO_6 nanojunction is an effective and stable VLD photocatalyst.

Photocatalytic activities of the above-mentioned photocatalysts can be further demonstrated by the degradation of some other organic compound, such as PCP that has no light absorption characteristics in the visible spectral region, as shown in Fig. 13. Obviously, upon visible-light irradiation, PCP is degraded more efficiently by AgBr-Ag-Bi_2WO_6 nanojunction system than by any other photocatalyst with single visible-light-active component, such as Bi_2WO_6, Ag-Bi_2WO_6 and AgBr-Ag-TiO_2 composite. More importantly, for both MX-5B and PCP degradation, it is discovered that pollutant degradation efficiencies by AgBr-Ag-Bi_2WO_6 nano-

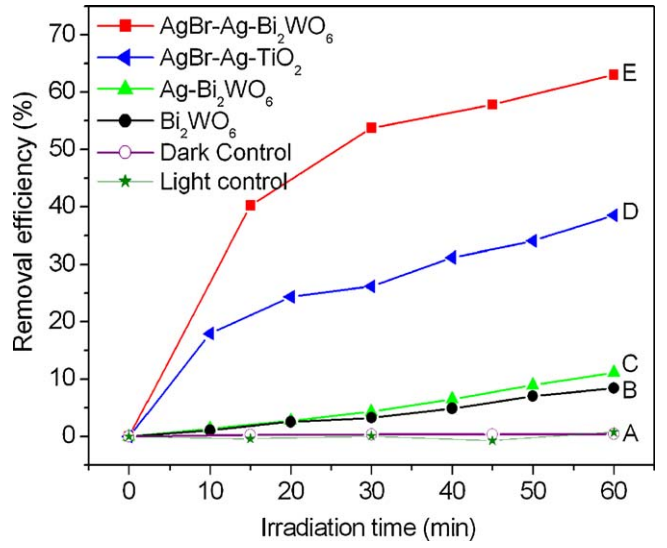

Fig. 13. The photodegradation of PCP (10 mg L^{-1}, 50 mL) in aqueous dispersions under visible-light irradiation containing photocatalysts with the same weight of each visible-light-active component (A) light control and dark control; (B) 9.55 mg Bi_2WO_6; (C) 9.7 mg Ag-Bi_2WO_6 containing 9.55 mg Bi_2WO_6; (D) 11.1 mg AgBr-Ag-TiO_2 composites containing 0.304 mg AgBr; (E) 10 mg AgBr-Ag-Bi_2WO_6 nanojunction containing 0.304 mg AgBr and 9.55 mg Bi_2WO_6.

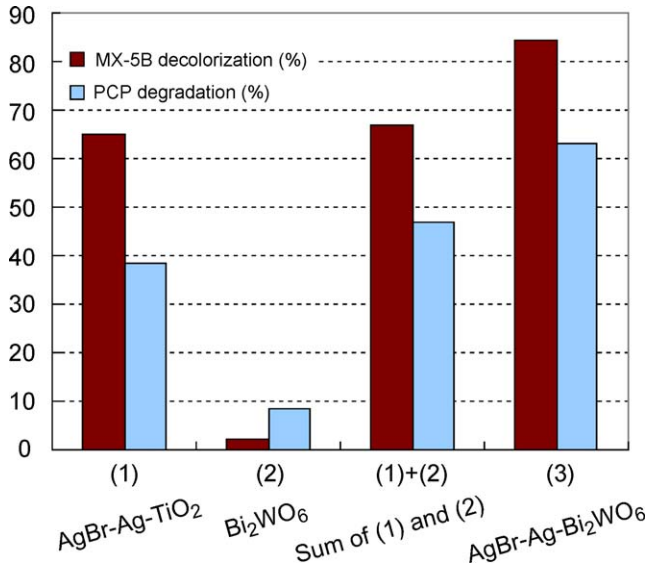

Fig. 14. The comparison of photocatalytic degradation efficiency of MX-5B and PCP by different photocatalyst containing the same weight of each visible-light-active component (AgBr or Bi_2WO_6) after 60 min of visible-light irradiation.

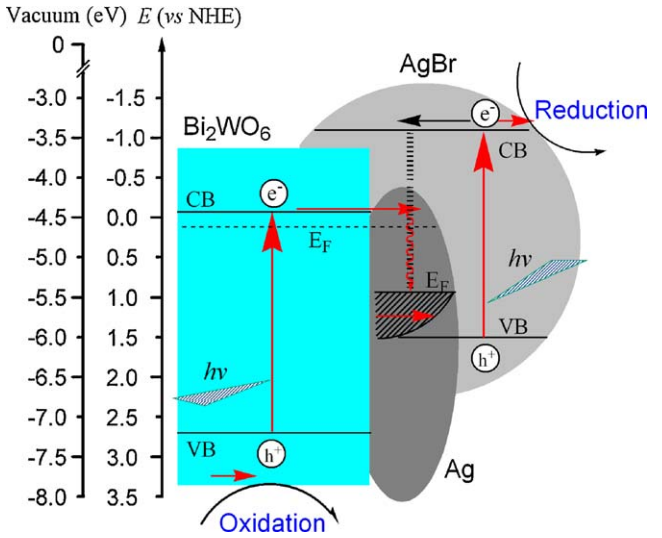

Fig. 16. Energy band diagram and photocatalytic scheme of the AgBr-Ag-Bi_2WO_6 nanojunction system.

junction are higher than total degradation efficiencies by two individual photocatalysts (AgBr-Ag-TiO_2 and Bi_2WO_6) containing the same weight of visible-light-active component (AgBr or Bi_2WO_6), as shown in Fig. 14. This result reveals that there is a synergic effect between the two-visible-light-active components (AgBr and Bi_2WO_6) in AgBr-Ag-Bi_2WO_6 nanojunction.

Using the PCP as organic pollutant target, we can also detect the change of TOC induced by AgBr-Ag-Bi_2WO_6 nanojunction and AgBr-Ag-TiO_2 composite under other identical conditions as a function of irradiation time (Fig. 15). It is clear that that TOC of the solution continuously decreases (Fig. 15), indicating that PCP steadily mineralized by both photocatalysts under visible-light irradiation. The loss of TOC via mineralization can be lowered more than the removed amount of organic pollutants because these large organic molecules are photooxidized to smaller organic intermediates such as aromatics, aldehydes, and ketones, and

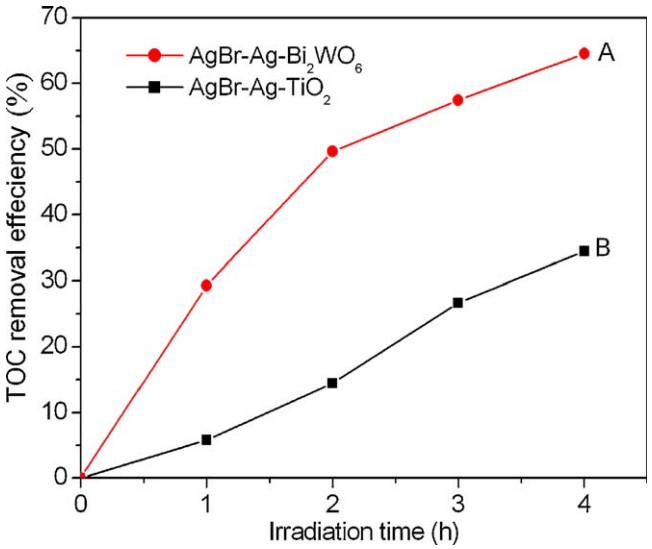

Fig. 15. The removal of TOC during the PCP photodegradation process (20 mg L^{-1}, 100 mL) in aqueous dispersions with 0.312 g of NaH_2PO_4 as buffer under visible-light irradiation: (A) 40 mg AgBr-Ag-Bi_2WO_6 nanojunction system containing 1.22 mg AgBr, (B) 45 mg AgBr-Ag-TiO_2 composite also containing 1.22 mg AgBr.

further degradation of these intermediates to CO_2 and H_2O may take place slowly. Moreover, mineralization of PCP within 4 h induced by AgBr-Ag-Bi_2WO_6 reaches 65% as shown in Fig. 15A, which is much higher than that (34.5%, as shown in Fig. 15B) induced by the AgBr-Ag-TiO_2 composite. This further confirms that the photocatalytic performance of AgBr-Ag-Bi_2WO_6 nanojunction with double visible-light active components (AgBr, Bi_2WO_6) is superior to that of AgBr-Ag-TiO_2 composite with single visible-light active component (AgBr).

The electronic structures and energy band of visible-light-response component AgBr and Bi_2WO_6 are widely studied by researchers [20,32–33]. On the basis of their energy band diagram, the photocatalytic process of AgBr-Ag-Bi_2WO_6 nanojunction system can be proposed, as shown in Fig. 16. Since both AgBr and Bi_2WO_6 can be excited by visible light and have different photoabsorption ranges, the conjunction of their photoabsorption can enhance the utilization of visible light and can broaden the range of visible-light photo-response. The photocatalytic reaction is initiated by the absorption of visible-light photons with energy equal or higher than the band-gap in either AgBr or Bi_2WO_6 semiconductors, which results in the creation of photogenerated holes in its valence band (VB) and electrons in its conduction band (CB). On one hand, CB-electrons (Bi_2WO_6) easily flow into metal Ag (electron transfer I: $Bi_2WO_6 \rightarrow Ag$) through the Schottky barrier because the CB (or the Fermi level) of Bi_2WO_6 is higher than that of the loaded metal Ag, which is consistent with the previous study on electron transfer from semiconductor (such as TiO_2) to metal (such as Ag, Au) [17,19,35–36]. This process of electron transfer I is faster than the electron–hole recombination between the VB and CB of Bi_2WO_6. Thus, plenty of CB-electrons (Bi_2WO_6) can be stored in Ag component, as was true with the previous study [35–36]. As a result, more VB-holes (Bi_2WO_6) with a strong oxidation power escape from the pair recombination and are available to oxidize the pollutants or OH^-, which explains the reason why the Ag-Bi_2WO_6 sample exhibits higher photocatalytic activity than the pure Bi_2WO_6 sample for the destruction of organic pollutant, as demonstrated in Figs. 7 and 13. On the other hand, since the energy level of Ag is above the VB of AgBr, VB-holes (AgBr) also easily flow into metal Ag (electron transfer II: $Ag \rightarrow AgBr$), which is faster than the electron–hole recombination between the VB and CB of AgBr. Thus, more CB-electrons (AgBr) with a strong reduction power can escape from the pair recombination and are available to reduce some absorbed compounds (such as O_2, H^+, etc.). Therefore,

simultaneous electron transfer I and II (that is, vectorial electron transfer of $Bi_2WO_6 \rightarrow Ag \rightarrow AgBr$) should occur as a result of visible-light excitation of both Bi_2WO_6 and AgBr, which is similar to suggestion in a report on the CdS-Au-TiO_2 three-component nanojunction system (vectorial electron transfer of $TiO_2 \rightarrow Au \rightarrow CdS$) [19]. In this vectorial electron-transfer process, metal Ag in AgBr-Ag-Bi_2WO_6 nanojunction system acts as a storage and/or recombination center for CB-electrons (Bi_2WO_6) and VB-holes (AgBr) and contributes to enhancing interfacial charge transfer and realizing the complete separation of VB-holes (Bi_2WO_6) and CB-electrons (AgBr). So this Z-scheme of AgBr-Ag-Bi_2WO_6 nanojunction can simultaneously and efficiently generate VB-holes (Bi_2WO_6) with a strong oxidation power and CB-electrons (AgBr) with a strong reduction power, explaining the high photocatalytic activity of the AgBr-Ag-Bi_2WO_6 nanojunction system compared with the sum of the activities of two photocatalysts (Bi_2WO_6 and AgBr-Ag-TiO_2), as proven in Fig. 14.

4. Conclusions

An all-solid-state AgBr-Ag-Bi_2WO_6 nanojunction system has been realized by using the facile deposition-precipitation method with Bi_2WO_6 sample as substrate, where both AgBr and Bi_2WO_6 are used as the VLD photochemical systems while Ag is used as electron-transfer system. The UV-Vis spectra indicate that the range of visible-light photo-response of AgBr-Ag-Bi_2WO_6 nanojunction system is broadened. The decolorization rate of MX-5B by AgBr-Ag-Bi_2WO_6 increases with the decrease of initial pH value and initial dye concentration. Importantly, this AgBr-Ag-Bi_2WO_6 nanojunction system shows much higher visible-light-driven (VLD) photocatalytic activity than a photocatalyst with single visible-light response component, such as Bi_2WO_6 nanostructures, Ag-Bi_2WO_6 and AgBr-Ag-TiO_2, for the degradation of an azo dye (MX-5B) and PCP. In particular, its photocatalytic activity is even higher than the sum of the activities of two photocatalysts (AgBr-Ag-TiO_2 and Bi_2WO_6) containing the same weight of visible-light component (AgBr or Bi_2WO_6). The energy band diagram scheme further suggests that in AgBr-Ag-Bi_2WO_6 nanojunction system, the vectorial electron transfer driven by the two-step excitation of both VLD components (AgBr and Bi_2WO_6) may be mainly responsible for its excellent VLD photocatalytic performance. Therefore, this work provides some insight into the design of new structures of multicomponent photocatalysts for enhancing VLD photocatalytic activity.

Acknowledgements

The project was supported by a research grant (CUHK4585/06M) of the Research Grant Council, Hong Kong SAR Government, allocated to P.K. Wong, J.C. Yu, C. Hu and C.Y. Chan. The authors also thank Prof. Chi Wu, Prof. To Ngai and Mr. Rui Deng of The Chinese University of Hong Kong for assisting in the measurements of zeta potentials of photocatalysts.

Appendix A. Supplementary data

Supplementary data associated with this article can be found, in the online version, at doi:10.1016/j.apcata.2009.05.028.

References

[1] M.R. Hoffmann, S.T. Martin, W. Choi, D.W. Bahneman, Chem. Rev. 95 (1995) 69–96.
[2] M. Fujihira, Y. Satoh, T. Osa, Nature 293 (1981) 206–208.
[3] J. Tang, Z.G. Zou, J.H. Ye, Angew. Chem. Int. Ed. 43 (2004) 4463–4466.
[4] R. Asahi, T. Morikawa, T. Ohwaki, K. Aoki, Y. Taga, Science 293 (2001) 269–271.
[5] J.M. Yu, W.K. Ho, J.G. Yu, H.Y. Yip, P.K. Wong, J.C. Zhao, Environ. Sci. Technol. 39 (2005) 1175–1179.
[6] J. Zhu, J. Ren, Y. Huo, Z. Bian, H. Li, J. Phys. Chem. C 111 (2007) 18965–18969.
[7] M. Hara, T. Kondo, M. Komoda, S. Ikeda, K. Shinohara, A. Tanaka, J.N. Kondo, K. Domen, Chem. Commun. 357 (1998) 357–358.
[8] W.F. Shangguan, A. Yoshida, J. Phys. Chem. B 106 (2002) 12227–12230.
[9] A. Kudo, K. Omori, H. Kato, J. Am. Chem. Soc. 121 (1999) 11459–11467.
[10] Z.G. Zou, J.H. Ye, K. Sayama, H. Arakawa, Nature 414 (2001) 625–627.
[11] H.G. Kim, D.W. Hwang, J.S. Lee, J. Am. Chem. Soc. 126 (2004) 8912–8913.
[12] B.B. Kale, J.O. Baeg, S.M. Lee, H. Chang, S.J. Moon, C.W. Lee, Adv. Funct. Mater. 16 (2006) 1349–1354.
[13] L.S. Zhang, J.L. Li, Z.G. Chen, Y.W. Tang, Y. Yu, Appl. Catal. A 299 (2006) 292–297.
[14] L.S. Zhang, W.Z. Wang, J. Yang, Z.G. Chen, W.Q. Zhang, L. Zhou, S.W. Liu, Appl. Catal. A 308 (2006) 105–110.
[15] L.S. Zhang, W.Z. Wang, Z.G. Chen, L. Zhou, H.L. Xu, W. Zhu, J. Mater. Chem. 17 (2007) 2526–2532.
[16] L.S. Zhang, W.Z. Wang, L. Zhou, H.L. Xu, Small 3 (2007) 1618–1625 (small is a journal name: http://en.wikipedia.org/wiki/Small_journal).
[17] S.X. Liu, Z.P. Qu, X.W. Han, C.L. Sun, Catal. Today 93 (2004) 877–884.
[18] H.G. Kim, P.H. Borse, W. Choi, J.S. Lee, Angew. Chem. Int. Ed. 44 (2005) 4585.
[19] H. Tada, T. Mitsui, T. Kiyonaga, T. Akita, K. Tanaka, Nat. Mater. 10 (2006) 782–786.
[20] C. Hu, Y.Q. Lan, J.H. Qu, X.X. Hu, A.M. Wang, J. Phys. Chem. B 110 (2006) 4066–4072.
[21] M.R. Elahifard, S. Rahimnejad, S. Haghighi, M.R. Gholami, J. Am. Chem. Soc. 129 (2007) 9552–9553.
[22] K.M. Pang, S. Ng, W.K. Chung, P.K. Wong, Water Air Soil Pollut. 183 (2007) 355–365.
[23] P. Tierno, W.A. Goedel, J. Phys. Chem. B 110 (2006) 3043–3050.
[24] J.F. Moulder, W.F. Stickle, P.E. Sobol, K.D. Bomben, Handbook of X-ray Photoelectron Spectroscopy, Perkin Elmer Corporation Physical Electronics Division, USA, 1992.
[25] C.M. So, M.Y. Cheng, J.C. Yu, P.K. Wong, Chemosphere 46 (2002) 905–912.
[26] N. Serpone, R. Terzian, C. Minero, E. Pelizzetti, Heterogeneous photocatalyzed oxidation of phenol, cresols, and fluorophenols in aqueous suspensions, in: C. Kutal, N. Serpone (Eds.), Photosensitive Metal-Organic Systems: Mechanistic Principles and Applications, American Chemical Society, New York, USA, 1993.
[27] K. Tanaka, K. Padermpole, T. Hisanaga, Water Res. 34 (2000) 327–333.
[28] C. Nasr, K. Vinodgopal, L. Fisher, S. Hotchandani, A.K. Chattopadhyay, P.V. Kamat, J. Phys. Chem. 100 (1996) 8436–8442.
[29] K. Vinodgopal, D.E. Wynkoop, P.V. Kamat, Environ. Sci. Technol. 30 (1996) 1660–1666.
[30] X. Yan, T. Ohno, K. Nishijima, R. Abe, B. Ohtani, Chem. Phys. Lett. 429 (2006) 606–610.
[31] Y. Liu, X. Chen, J. Li, C. Burda, Chemosphere 61 (2005) 11–18.
[32] J. Belloni, M. Treguer, H. Remita, R.D. Keyzer, Nature 402 (1999) 865–867.
[33] X. Zhao, Y. Wu, W.Q. Yao, Y.F. Zhu, Thin Solid Films 515 (2007) 753–4757.
[34] H. Fu, C. Pan, W. Yao, Y. Zhu, J. Phys. Chem. B 109 (2005) 22432–22439.
[35] T. Hirakawa, P.V. Kamat, J. Am. Chem. Soc. 127 (2005) 3928–3934.
[36] V. Subramanian, E.E. Wolf, P.V. Kamat, J. Am. Chem. Soc. 126 (2004) 4943–4950.